Test Plan for Investigation of Hydrogen Generation in SNF Canisters

Spent Fuel and Waste Disposition

Prepared for
US Department of Energy
Spent Fuel and Waste Science and Technology

A.L. d'Entremont
R.L. Kesterson
R.L. Sindelar

March 26, 2021
Milestone No. M4SF-21SR010203044
SRNL-STI-2021-00171 Revision 0

DISCLAIMER

This work was prepared under an agreement with and funded by the U.S. Government. Neither the U.S. Government or its employees, nor any of its contractors, subcontractors or their employees, makes any express or implied:

1) warranty or assumes any legal liability for the accuracy, completeness, or for the use or results of such use of any information, product, or process disclosed; or
2) representation that such use or results of such use would not infringe privately owned rights; or
3) endorsement or recommendation of any specifically identified commercial product, process, or service.

Any views and opinions of authors expressed in this work do not necessarily state or reflect those of the United States Government, or its contractors, or subcontractors.

Prepared by
Savannah River National Laboratory
Aiken, South Carolina 29808

Savannah River National Laboratory®
OPERATED BY SAVANNAH RIVER NUCLEAR SOLUTIONS

EXECUTIVE SUMMARY

This report presents a test plan to investigate radiolytic hydrogen generation in spent nuclear fuel (SNF) canisters containing Zr-based cladding materials. The initial primary contributor to the generation of radiolytic hydrogen is estimated to be the residual physisorbed water on the ZrO_2 film, post-dryout. Over the longer term the primary hydrogen source is associated with the aluminum hydroxides and water vapor.

The proposed testing to be conducted in FY22 would consist of lab-scale testing on non-radioactive surrogates of oxidized ZIRLO tubing and unalloyed zirconium using a miniature steel canister ("mini-canister") designed to allow intermittent, in-situ sampling of the canister gas during irradiation. The mini-canister approach for irradiation with in-situ monitoring system was used in a recent and on-going study [McNamara and Verst, 2020a & 2020b; Verst et al., 2021] to measure radiolytic hydrogen generation from aluminum SNF cladding surrogate materials. This proposed testing will form part of the overall materials performance evaluation of the commercial SNF-in-canister system and is part of the technical bases for their continued safe dry storage.

The proposed test plan draws on previous radiolysis testing focused on aluminum-clad spent nuclear fuel (research reactor fuel) as well as the previous analysis, "Evaluation of Hydrogen Generation in High Burnup Demonstration Dry Storage Cask" [d'Entremont et al., 2020b], which provided a best-estimate evaluation of residual water content (post-dryout) in the High Burnup (HBU) LWR Spent Fuel Demonstration project TN-32 cask and evaluated the expected radiolysis of the residual water, including free, physisorbed, and chemisorbed water in the sealed cask, based on literature data and models.

Under gamma radiation, radiolytic breakdown of water remaining in a canister (free, physisorbed, or chemisorbed) causes the generation of hydrogen gas (H_2). SNF fuel assemblies, clad in zirconium alloys, provide a large surface area to host surface-adsorbed water (physisorbed water). Various other components in the cask, including stainless steel and aluminum structural components and aluminum neutron absorbers also contribute to the total water inventory and radiolytic H_2 generation in an SNF canister. Water adsorbed to the ZrO_2 on the cladding surface may experience accelerated radiolysis compared to free water due to energy exchange with the oxide. In addition, water decomposed by radiolysis may be replenished by water vapor in the canister gas, providing a mechanism for accelerated radiolysis of the free water. The previous simplified analysis [d'Entremont et al., 2020b] predicted that radiolysis of physisorbed water on the Zr-alloy components would dominate the short-term H_2 generation due to these factors.

The proposed test plan therefore focuses on the contribution associated with the Zr-alloy components, i.e., surface-adsorbed water as well as interactions with free water vapor present in the gas phase. The radiolytic hydrogen generation will be empirically measured using in-situ gas sampling over the course of the irradiation to track the H_2 and O_2 concentrations and relative humidity in the canister gas. In the absence of consensus standard testing methods for radiolysis, empirical measurement in a test system (the mini-canister) similar to the SNF-in-canister environment to control for environmental effects is expected to provide the best data for predicting hydrogen generation for actual SNF-in-canister.

This testing will improve understanding of radiolytic breakdown of water on Zr-based components and the resulting H_2 generation. The experimentally measured hydrogen generation rates and temporal evolution of the H_2 concentration can be used to refine estimates and predictive models for full-scale SNF canisters.

Upon the successful completion with the surrogate materials, additional correlation testing is recommended in FY23 using actual service-exposed cladding samples from the Sibling Pin program.

This report fulfills the M4 milestone M4SF-21SR010203044, *Test Plan for Investigation of Hydrogen Generation in SNF Canisters* under Work Package Number SF-21SR01020304.

ACKNOWLEDGEMENTS

The authors gratefully acknowledge the support of Ned Larson, U.S. Department of Energy, Office of Nuclear Energy, Office of Spent Fuel and Waste Disposition, Office of Spent Fuel & Waste Science and Technology, for his office's sponsorship of this work, and supported by Control Account Manager Sylvia Saltzstein from Sandia National Laboratories and deputy CAM Brady Hanson from the Pacific Northwest National Laboratory. The authors thank Charles Bryan of Sandia National Laboratories for his review comments in the course of this work including those on the physisorption phenomena for oxides.

TABLE OF CONTENTS

1. INTRODUCTION 13

2. WATER RADIOLYSIS AND HYDROGEN GENERATION 13
2.1. G_{H2} Values ..... **Error! Bookmark not defined.**
2.1.1. Temperature ..... **Error! Bookmark not defined.**
2.1.2. Cover Gas ..... **Error! Bookmark not defined.**
2.1.3. Alloy Surface and Substrate ..... **Error! Bookmark not defined.**
2.1.4. Gamma Dose and Initial Transition Effects 16

3. ENVIRONMENT OF ZIRCONIUM-CLAD SNF IN CANISTER 17
3.1. Temperature 18
3.2. Strongly Physisorbed/Chemisorbed Surface Water 18
3.2.1. Zr-Alloy Oxides 18
3.2.2. Stainless-Steel Surfaces 19
3.3. Water Vapor 20
3.4. SNF Drying Procedure 20

4. TEST OBJECTIVES AND APPROACH 20
4.1. Test Objectives 20
4.2. Test Approach 21
4.2.1. Zirconium samples and ZIRLO samples 21
4.2.2. Drying effectiveness 21
4.2.3. ZrO_2 impact on radiolysis of adsorbed water 21
4.2.4. Energy transfer from oxide and/or metal 22
4.2.5. Physisorbed water replenishment from humidity 22

5. EXPERIMENTAL SETUP AND METHODS 22
5.1. Gamma Irradiator 22
5.2. Mini-Canister and Instrumentation System 23
5.2.1. Mini-Canister 23
5.2.2. Sampling Instrumentation 23
5.2.3. Helium Backfill 24
5.2.4. Canister Heating for Radiolysis at Elevated Temperature 24
5.3. Zr-alloy samples 24
5.3.1. Lab-prepared surrogate samples 24
5.3.2. Service-exposed materials (FY23) 26
5.3.3. Sample characterization 26
5.4. Drying 26
5.5. Model estimates for mini-canister setup 27

6. PRELIMINARY TEST MATRIX 28

7. CONCLUSIONS 28

8. REFERENCES 29

This page is intentionally left blank.

LIST OF TABLES

No table of figures entries found.

This page is intentionally left blank.

LIST OF FIGURES

Figure 2-1. Temperature Effect on G_{H2} [Elliot, 2009] 14

Figure 2-2. Effect of Nb^{+5} doping of ZrO_2 on the radiolytic H_2 production from adsorbed water [Petrik et al., 2001] 16

Figure 2-3. Representative data points from [Wittman, 2013] obtained at multiple dose rates plotted as a function of dose, with a power-law fit (G in units of molecules of H_2 per 100 eV energy deposited) [d'Entremont et al., 2020b] 17

Figure 3-1. Radial distribution of system component temperatures at the axial location of Peak Cladding Temperature for initial storage conditions (as of 7/31/2017) [Fort, 2019] 18

Figure 3-2. Schematic of adsorbed water on stainless steel [Dylla, 2006] 20

Figure 5-1. Schematic of coupon assembly design from [McNamara and Verst, 2020b], viewed from the top. 25

Figure 5-2. Photos of aluminum coupon assembly and corresponding mini-canister from [McNamara and Verst, 2020b]. The proposed sample design will be similar for the oxidized unalloyed Zr material, but axially shortened to accommodate thermal insulation around the mini-canister. Oxidized ZIRLO tubes would be used in a separate mini-canister. 25

This page is intentionally left blank.

ACRONYMS

DOE	Department of Energy
FY	Fiscal year
G_{H2}	Number of hydrogen molecules created per unit of energy deposited in the system
Gy	Gray [1 Gy = 100 Rad = 1 Joule per Kg = 6.2415 x 10^{12} MeV per kg]
HBU	High Burnup
kGy	kiloGray
LWR	Light Water Reactor
NE	DOE, Office of Nuclear Energy
NE-SFWST	Office of Nuclear Energy, Spent Fuel and Waste Science and Technology
ppmv	part per million, by volume
RH	Relative Humidity
SEM	Scanning Electron Microscopy
SNF	Spent Nuclear Fuel
SRNL	Savannah River National Laboratory

This page is intentionally left blank.

1. INTRODUCTION

Residual water (post-drying and sealing) in a spent nuclear fuel (SNF) canister can result in corrosion and radiolysis that can affect the spent nuclear fuel and canister internal structural materials [CNWRA 2013, Shukla et al, 2019, ASTM C1553-16]. Recent work [Bryan et al., 2019a] showed that inadvertent free water (~100 ml) may remain following drying even with a dryness criterion of 3 torr pressure limit following a 30-minute hold after active drying is complete[a] and measured ~500 ppmv of H_2 after 12 days post-dryout in the High Burnup (HBU) Demonstration Cask.

An important phenomenon is the radiolysis of the residual free water creating H_2 and H_2O_2, an oxidizing specie that is expected to quickly break down on surfaces and cause oxidation reactions with the cladding, exposed fuel, and other materials in the canister. With radiolysis of the residual free water and consumption of oxygen, hydrogen gas is the expected net product in the canister free volume. Characterization of the rate of radiolysis is important to estimate the impacts of residual water.

This present work supplements the previous evaluation of radiolytic hydrogen in SNF canisters (which used the HBU Demo Cask as a demonstration case) [d'Entremont et al., 2020b]. A test plan to investigate the hydrogen generation associated with water interacting with Zr-based materials under gamma irradiation and to provide data that can be used in further modeling for predicting hydrogen content in SNF canisters is outlined. A sealed, stainless-steel miniature canister in an ^{60}Co irradiator is used as the primary test system to provide an environmental configuration closely analogous to an SNF-in-canister dry storage environment.

Radiolysis and hydrogen generation are part of the present investigations regarding the consequences of inadvertent water (post-dryout) in the Office of Nuclear Energy, Spent Fuel and Waste Science and Technology (NE-SFWST) campaign. Hydrogen content is a measure of the extent of radiolysis that has occurred in the canister and an indirect indicator of the residual water in a canister. It is recognized that the generation of hydrogen from radiolysis in an SNF canister does not pose a flammability concern if the oxygen concentration remains sufficiently low (< 5 vol. %) [Sindelar, et al, 2020].

2. WATER RADIOLYSIS AND HYDROGEN GENERATION

Our previous evaluation [d'Entremont et al., 2020b] included literature review on water radiolysis with a focus on the G_{H2} values under various conditions relevant to SNF-in-canister. Gettering of hydrogen by reactions with the fuel cladding and other zirconium-alloy components and chemical back reactions were

[a]The U.S. NRC evaluates the drying adequacy for dry storage packages prior to backfilling with inert gas [taken from NUREG-2215]:

> "The following examples illustrate the accepted methods for cask draining and drying in accordance with the recommendations of PNL-6365 (Knoll and Gilbert 1987):
>
> • The DSS confinement cavity should be drained of as much water as practicable and evacuated to less than or equal to 4.0x10-4 MPa (4 millibar, 3.0 mm Hg or Torr). After evacuation, adequate moisture removal should be verified by maintaining a constant pressure over a period of about 30 minutes without vacuum pump operation (or the vacuum pump is running but it is isolated from the cask with its suction vented to atmosphere). The DSS confinement cavity is then backfilled with an inert gas (e.g., helium) for applicable pressure and leak testing. Care should be taken to preserve the purity of the cover gas and, after backfilling, cover gas purity should be verified by sampling."

not considered. Key predictions of that analysis were that the short-term hydrogen generation would be dominated by the radiolysis of water adsorbed to Zr-alloy surfaces and that the amount of hydrogen generated by this mechanism was heavily dependent on whether or not the surface-adsorbed water could be replenished by water vapor [d'Entremont et al., 2020b]. Information from the previous literature relevant to the narrower scope of the current test plan is included here.

G_{H2} represents the production rate of hydrogen molecules during radiolysis of hydrogen-containing substances and is reported in units of molecules per radiation dose, typically molecules of H_2 per 100 eV or µmol H_2 per joule (1 µmol/joule = 9.63 molecules/100 eV).

Gamma radiolysis of H_2O has been studied extensively. The radiolysis results in the rapid formation of molecules, atoms, ions, and radicals which react to form stable components (H_2, H_2O_2, and H_2O). The relative quantities of the stable components and the resulting G-values depend on the system/environment where radiolysis occurs and are not constant values across differing systems. As a result, measuring G_{H2} values in an environment closely resembling that of the SNF-in-canister is important for enabling predictions of the hydrogen generation in a canister.

2.1. Temperature

Elliot [Elliot, 2009] summarized data regarding the effect of temperature on G_{H2} from several literature sources. The summary is shown in Figure 2-1 and indicates an increasing G_{H2} with temperature. Some of the data points were generated in water with added solutions which can impact the G-value by scavenging and reacting with other species from the radiolysis. The trend line follows the data that was extrapolated to zero concentration and is consistent with the typical G_{H2} value from Spinks of 0.45 molecules/100 eV. The trend line follows equation {1} and has a G_{H2} value of 0.44 molecules/100 eV at 23°C and 0.56 molecules/100 eV at 250°C for the system used to determine the values. The temperatures within the fuel element storage cask vary and will decrease over time but, based on the data in Figure 2-1, the G_{H2} value for free water is expected to have relatively small temperature-related variation over the temperature range relevant for the canister (~< 275°C) and is expected to remain below 0.6 molecules/100 eV.

$$G_{H2} = 0.419 + 8.721\times10^{-4}\ T - 4.971\times10^{-6}\ T^2 + 1.503\times10^{-8}\ T^3 \qquad \{1\}$$

where T is the temperature in °C and G_{H2} is given in molecules/100 eV.

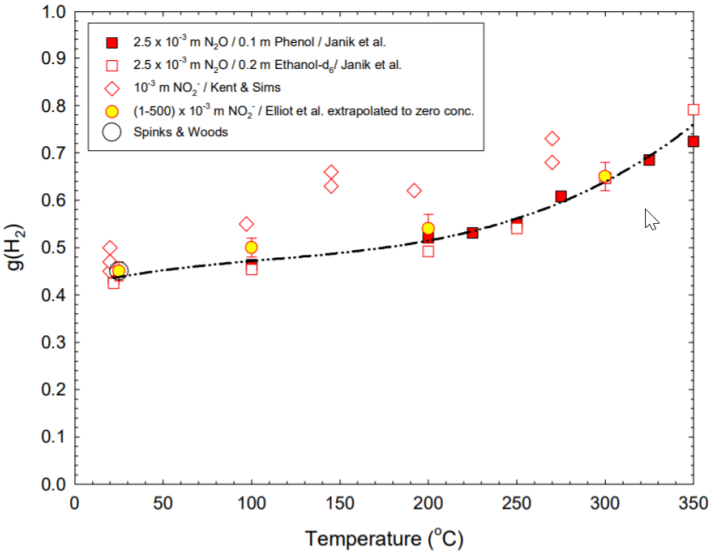

Figure 2-1. Temperature Effect on G_{H2} [Elliot, 2009]

For radiolysis of surface-adsorbed water, temperature could potentially affect not only the radiolysis process itself but also the amount of water adsorbed to the surface. A previous study [Garibov et al., 2015] found that the G_{H2} of water adsorbed to ZrO_2 powder increased with increasing temperature.

2.2. Cover Gas

The net hydrogen generation can also be affected by the gas environment. Recent work on radiolysis of physisorbed and chemisorbed water on aluminum coupons involved irradiation of nominally identical samples sealed in ampoules with air, N_2, or argon cover gas [Parker-Quaife et al., 2019]. They observed a significantly greater initial yield of H_2 for argon compared to N_2 and no detectable H_2 under air, which was attributed to scavenging of free radicals by O_2 in the air [Parker-Quaife et al., 2019]. Preliminary comparisons of argon versus helium demonstrated an impact of cover gas even among noble gases, with irradiation under helium producing up to 58% greater yield of radiolytic H_2 compared to argon for both "pristine" coupons (i.e., uncorroded and assumed to bear only physisorbed water) and coupons with an oxyhydroxide film [Parker-Quaife and Horne, 2020].

For the actual SNF cask or mini-canister test setup, the environment is relatively pure with only helium cover gas and water vapor, so no significant impact on G_{H2} values from reactions with the cover gas are expected (except possible minor effects from small amounts of residual air and hydrocarbons). However, literature G_{H2} values will depend on the cover gas used while measuring them, so it is important to have values measured under the intended cover gas. Since the mini-canister setup is designed to replicate the cask gas environment, the measured G_{H2} values should be representative of the full-scale system.

2.3. Alloy Surface and Substrate

Elliott [Elliott, 2009], discussing radiolysis of water, reported that the substrate where water is physisorbed, chemisorbed, or retained as radicals has an impact on the hydrogen production rate and corresponding G_{H2}. For the current work, the relevant surfaces are zirconium alloy covered by ZrO_2 and the stainless steel of the mini-canister. In many SNF canister systems, aluminum surfaces will be present and will also be important contributors to radiolytic hydrogen. Studies of radiolysis and the associated G_{H2} values on aluminum surfaces (both pristine and bearing significant aluminum oxyhydroxide layers) are in progress as part of the technology development to enable dry storage of DOE-owned aluminum spent nuclear fuel [Parker-Quaife, 2020].

There have been numerous reports on radiolysis of water in contact with ZrO_2 powders and crystals and evaluations of the effects of surface physisorbed/chemisorbed water. Garibov [Garibov et al., 2015] reported a G_{H2} value of 2.14 molecules/100 eV for adsorbed water on nano-ZrO_2 powder at a temperature of 300 K (with increasing G_{H2} as the temperature increased). Petrik et al. [Petrik et al., 2001] also observed high G_{H2} for water adsorbed on ZrO_2 powders compared to pure water. Doping of ZrO_2 powders was demonstrated to be able to significantly reduce (for Nb^{+5}, Figure 2-2) or increase (for Li^+ or Rb^+) the hydrogen production at very low percent mass of the dopant [Petrik et al., 2001]. Lattice defects were postulated to play a role in this. Zr alloys used for SNF cladding contain alloying elements that could impact the radiolytic yield in similar ways. ZIRLO and M5 include 1% Nb as an alloying additive, so the resulting oxide will contain Nb along with other precipitates that produce lattice defects. Zirc-4 does not include Nb, but does include Sn, Cr, and Fe, which will also result in lattice defects.

For test optimization, the initial irradiations in the proposed testing will use oxidized pure Zr samples, and the oxide will not have significant precipitates or alloying elements. Correlating tests will be performed using oxidized ZIRLO samples and will provide information on the effects of alloy elements.

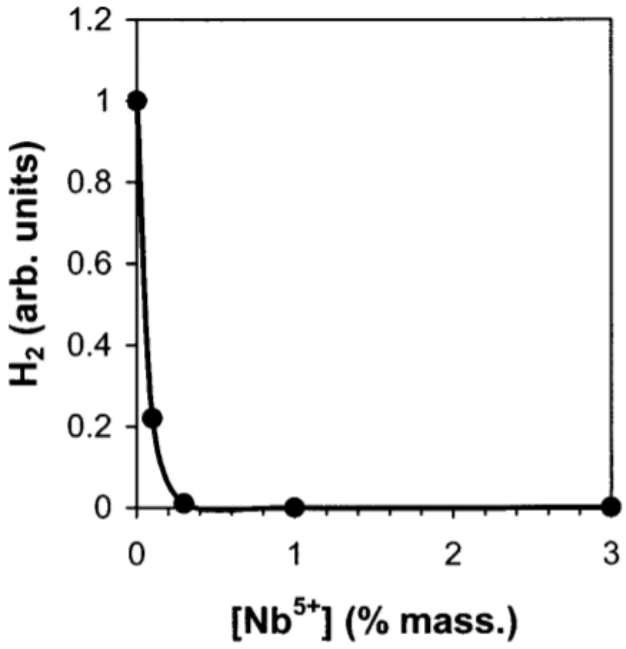

Figure 2-2. Effect of Nb^{+5} doping of ZrO_2 on the radiolytic H_2 production from adsorbed water [Petrik et al., 2001]

For water adsorbed on ZrO_2, the previous evaluation [d'Entremont et al., 2020b] assumed the energy deposited in the oxide mass (in addition to that deposited in the physisorbed water directly) contributed to the radiolysis of water adsorbed on the oxide. As a result, the initial radiolytic H_2 generation rate and the amount of H_2 generated in the first 12 days for the HBU Demo Cask was predicted to be overwhelmingly dominated by that associated with the Zr surfaces due to the assumed energy transfer from the thick oxide mass greatly accelerating the radiolysis of the adsorbed water [d'Entremont et al., 2020b].

2.4. Gamma Dose and Initial Transition Effects

The long-term, steady-state G-values are critical data when evaluating water radiolysis in dry storage systems. The G-values calculated from initial irradiation doses can be/are different than the long-term doses when a quasi-steady-state condition evolves including back reactions and environmental effects. Re-plotting representative G-values measured by Arkhipov [Arkhipov, 2007] in water vapor for different radiation dose rates and irradiation times showed that G_{H2} obtained for different dose rates fall along the same curve when plotted as a function of accumulated dose, indicating that G_{H2} is a function of the total accumulated dose (in Gy) and not the dose rate (Gy/s) [d'Entremont et al., 2020b]. The trend line was fitted with a power-law fit that decreased from an initial maximum and approached a consistent G_{H2} value with increasing dose (extrapolated as G_{H2} = 0.45 molecules/100 eV at a dose of 1000 kGy in this case, similar to values typically used for H_2 yield from water). It is postulated that mechanistically the behavior may not follow a power law, so this fit may not extrapolate to accurately represent the G-values at very high dose levels but for moderate dose levels the data does indicate a plateauing of G_{H2} near the typically reported values.

The radiation energy level can also affect the measured G-value [Le Caër, 2011; Kabakchi et al., 2013; Wang, 2013]. The relevant radiation for SNF is low-LET gamma ray energy. Here, a Co^{60} irradiator will be used to provide gamma irradiation analogous to that for SNF-in-canister. The gamma decay energy associated with Co^{60} (>1 MeV) is larger than that of Cs^{137} (0.66 MeV), a major gamma radiation source from spent fuel.

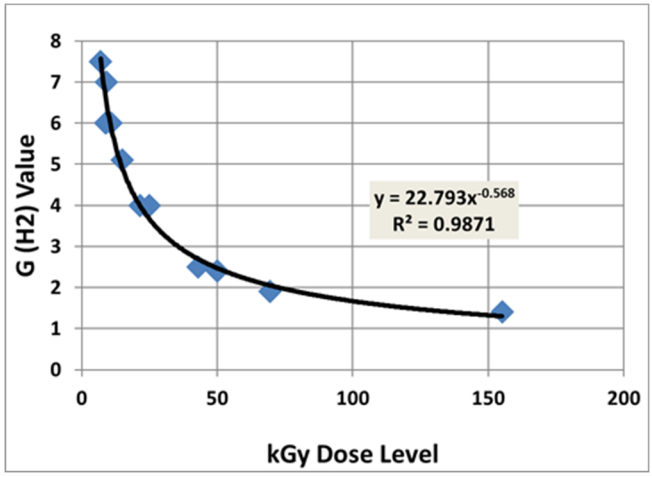

Figure 2-3. Representative data points from [Wittman, 2013] obtained at multiple dose rates plotted as a function of dose, with a power-law fit (G in units of molecules of H_2 per 100 eV energy deposited) [d'Entremont et al., 2020b]

3. ENVIRONMENT OF ZIRCONIUM-CLAD SNF IN CANISTER

Our previous evaluation [d'Entremont et al., 2020b] estimated potential inventories of residual water (free, physisorbed, and chemisorbed) and radiolytic H_2 generation therefrom in a sealed and dried SNF-in-canister system, using the High Burnup Demo storage cask from North Anna [Bryan et al, 2019a] as a specific example for a quantitative estimate. This analysis [d'Entremont et al., 2020b] predicted that water adsorbed on the fuel rod surface, water vapor, and hydrated oxides on the aluminum rails were the only potentially significant contributors to H_2 radiolysis in the HBU Demo Cask, and that the short-term hydrogen generation rate would be dominated by radiolysis associated with the Zr-alloy surfaces.

The present test plan therefore focuses on experimentally investigating radiolytic H_2 production associated with adsorbed water on Zr-alloy surfaces to refine these predictions. This includes assessing the impact of the water vapor in the canister environment and its potential to replenish the adsorbed water on ZrO_2. The tests will use a stainless-steel miniature canister in order to closely replicate the environment of the SNF-in-canister system.

SNF canisters are loaded with spent fuel assemblies underwater. After loading of fuel assemblies into the storage cask, the canister is prepared for drying and long-term storage by draining the water and performing numerous blowdowns to further enhance the water removal, followed by drying via a sequence of vacuum and hold conditions and a backfill with helium (e.g., the HBU Demo Cask was backfilled to an at-temperature pressure of 32 psi = 2.2×10^5 Pa) [Bryan et al, 2019a].

The loading of SNF into dry storage casks and the subsequent drying operation can leave small amounts of residual water in the sealed casks, as assessed in [d'Entremont et al., 2020b]. The relevant water sources for the current experimental campaign are:

a) Surface-adsorbed (physisorbed/chemisorbed) water on Zr-alloy and stainless-steel (canister) surfaces and

b) Water vapor in the canister gas space.

Other potential water reservoirs in a sealed SNF dry storage canister include liquid water, water trapped in pores of oxide or crud, and water chemically bound in hydrated oxides, but these water inventories are outside the scope of the current test plan. Although significant quantities of hydrated oxides are known to form on aluminum surfaces such as research-reactor fuel cladding [d'Entremont et al., 2020c], Zr-alloy

components and their attendant ZrO_2 surface films are not expected to form significant amounts of hydrated oxide.

3.1. Temperature

The stored fuel and adjacent structures are relatively hot as shown in the temperature models for the HBU cask from [Fort, 2019] (Figure 3-1). The temperature of the materials in the canister affects the amount of surface-adsorbed water and could affect the radiolysis and/or back-reactions governing the amount of H_2 generated. Surface-adsorbed water can have varying adsorption energies, often with the first few monolayers strongly bound to the surface and additional, more weakly bound layers forming on top in equilibrium with the humidity. The weakly physisorbed water and the strongly physisorbed water are driven off of the surface at different temperatures. The peak temperatures of fuel and adjacent structures of the dried SNF-in-canister are in the 200–250°C range per Figure 3-1.

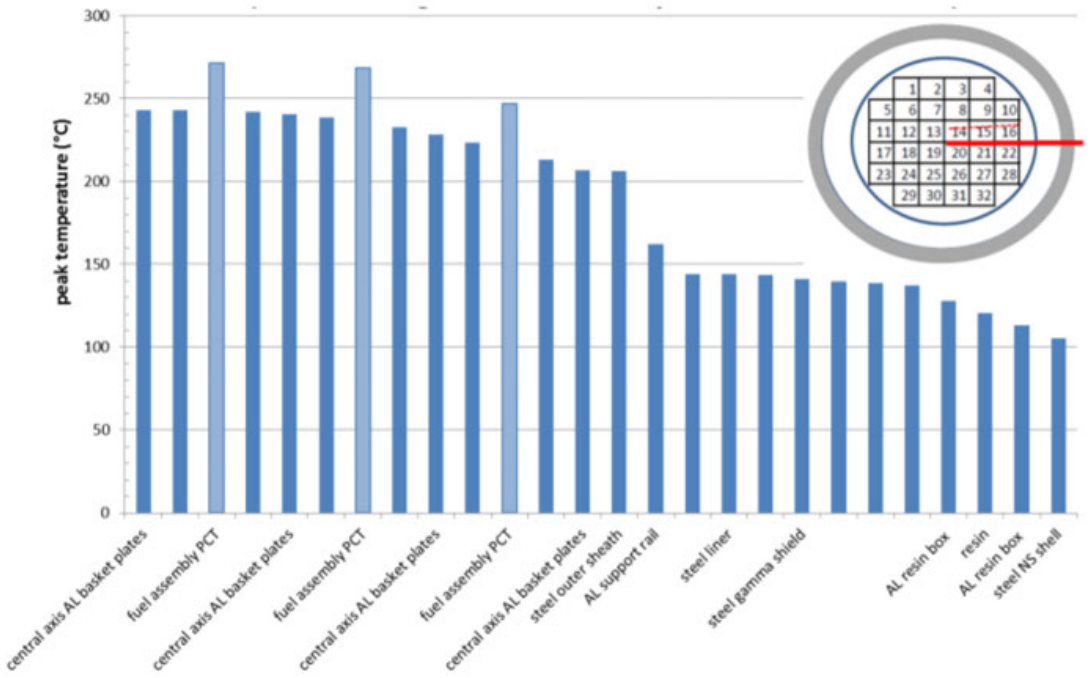

Figure 3-1. Radial distribution of system component temperatures at the axial location of Peak Cladding Temperature for initial storage conditions (as of 7/31/2017) [Fort, 2019]

3.2. Strongly Physisorbed/Chemisorbed Surface Water

In this study, the term "chemisorbed water" is used for water incorporated chemically in hydrated oxides such as aluminum (oxy)hydroxides, as opposed to "physisorbed water" that is adsorbed (strongly or weakly) at the surface of the oxide. No significant formation of hydrated oxides and thus no significant chemisorbed water are expected on stainless-steel or Zr-alloy components. Surface-adsorbed water for steels and zirconium oxide here refers to molecularly thin surface layers of H_2O that are bonded via surface radicals and/or a very thin layer of hydrated oxide.

3.2.1. Zr Oxides

The zirconium oxide on the surface of the fuel rods is expected to host surface-adsorbed water. The depth of any truly hydrated zirconium oxide (i.e., chemisorbed water), if present, is expected to be at most only a few molecular layers and not representative of the bulk of the zirconium oxide.

Many investigators [Agayev, 2017; Skotnicki, 2015; Petrik, 2001; Holmes, 1974; Köck, 2016; for example] evaluated the strong physisorption/chemisorption of water on ZrO_2 using powders, thin lab-grown oxides, and some with added solutions for scavenging radiolysis species. Hydroxyls are reported to form at the oxide surface when water is present, and these hydroxyls act as anchors for one or a few molecular layers of adsorbed water. This is a surface effect that does not involve water chemically incorporated throughout the bulk of the oxide. Thus, the adsorbed water on Zr components is relatively limited even with large surface area.

The area of a single fuel rod is given as 0.115769 m^2, with 264 rods in an assembly [Bryan et al., 2019b], and the mass of a single-molecule-thick physisorbed water layer is reported to be between 0.187 and 0.3 mg/m^2 [Petrik, 2001; Wertsching, 2007]. A single monolayer of water on all fuel rods in an assembly is thus estimated to be between ~6.7 and 9.2 mg of physisorbed/chemisorbed water per assembly. Bryan [Bryan et al., 2019b] estimated the surface-adsorbed water on the fuel rod oxide surface to be about 12 mg per SNF assembly (all fuel rods plus other components) based on an empirical adsorbed water loading on ZrO_2 of 0.25 mg/m^2. The rate of water removal during cask drying is not known, so some of this water may be removed during drying. However, experimental data suggested that the adsorbed water binds strongly to ZrO_2 and thus may remain even after reaching elevated temperatures [Bryan et al., 2019b].

3.2.2. Stainless-Steel Surfaces

Per Dylla [Dylla, 2006], the strongly physisorbed/chemisorbed water on stainless steel comprises less than a monolayer on the actual surface area but is equivalent to about five monolayers when considering the nominal/macroscopic surface area, as illustrated in Figure 3-2. Additional layers of physisorbed water are weakly bound and reported to easily desorb in vacuum. It is expected that the weakly physisorbed water and at least some of this strongly physisorbed/chemisorbed water on the steel would be depleted during the drying operation.

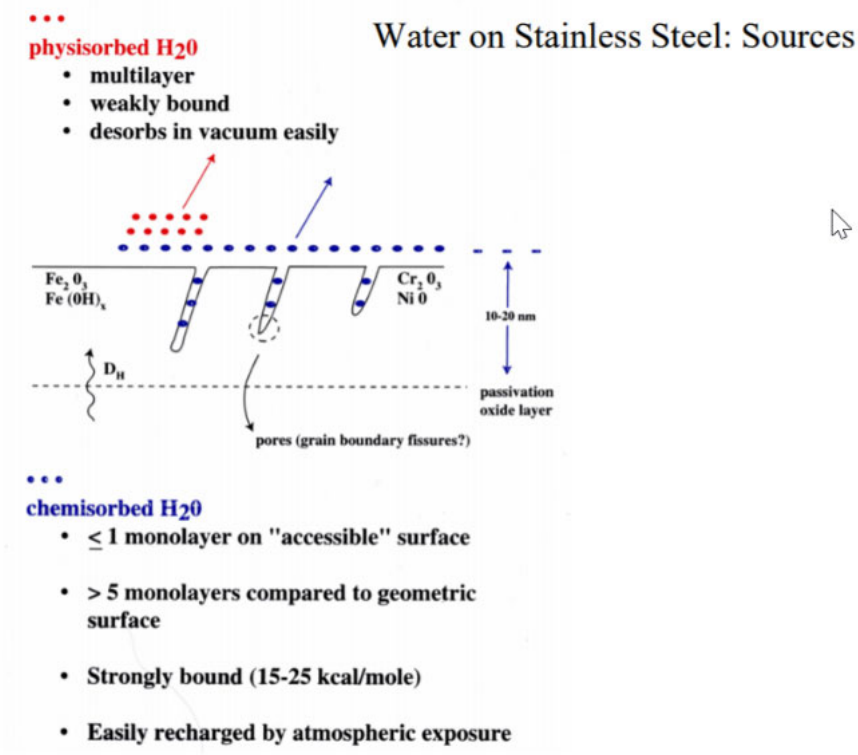

Figure 3-2. Schematic of adsorbed water on stainless steel [Dylla, 2006]

3.3. Water Vapor

Bryan [Bryan et al, 2019a] measured water vapor in the sampled HBU Demo Cask gas at a level of 17,400 ppmv at 65°C after 12 days post-closure. This vapor content was estimated to correspond to less than 10% RH at the temperatures inside the cask [Bryan et al., 2019a].

A key factor in estimating the hydrogen generation is the assumption of how the water vapor and the surface-adsorbed water on various components interact. If there is rapid exchange between the water vapor and physisorbed water, then the water vapor provides a reservoir for replenishing water on the surfaces as it is depleted by radiolysis, including providing a potential medium for transferring adsorbed water from surfaces with lower radiolysis rates to those with higher radiolysis rates. The amount of water radiolysis predicted to occur on the Zr surfaces is strongly dependent on whether its physisorbed water is replenished from the humidity in the gas or not [d'Entremont et al., 2020b].

3.4. SNF Drying Procedure

SNF canisters are loaded with spent fuel assemblies underwater. After loading of fuel assemblies into the storage cask, the canister is prepared for drying and long-term storage by draining the water and performing numerous blowdowns to further remove free water. The drying process involves a sequence of vacuum and hold conditions with the cask internal volume being brought to an initial 55 Pa (0.41 Torr) vacuum [Bryan et al, 2019a]. The vacuum drying time for the HBU cask was less than 9 hours [Fort et al., 2019]. Drying completion is verified by evacuating and sealing the canister, and monitoring the rise in pressure due to water evaporation or desorption; the pressure must remain below 3 Torr after 30 minutes for the canister to be considered dry [Bryan et al., 2019b]. After drying is completed, the canister is backfilled with helium [Bryan et al, 2019a].

During vacuum drying, the fuel is heated by its own decay heat, thermally insulated by the surrounding vacuum. Fort et al., 2019, modeled the temperature during the drying process for the HBU Demo Cask and predicted peak cladding temperatures during vacuum drying could reach between 217°C and 266°C based on anticipated drying times of 10–36 hours.

4. TEST OBJECTIVES AND APPROACH

4.1. Test Objectives

The objective of this study is to obtain empirical data to refine assumptions and values of critical parameters used in the radiolysis analysis [d'Entremont, 2020b]. Primary objectives include:

1. Measuring G_{H2} of water adsorbed on Zr-based components in a canister-relevant environment (ZrO_2 surface film, helium cover gas, and steel container, dried analogously to SNF-in-canister),
2. Assessing impact of energy transfer from the ZrO_2 and/or metal to the adsorbed water in accelerating radiolysis, and
3. Confirming whether replenishment of physisorbed water from water vapor occurs.

Additional experimental targets in support of a more refined predictive model include:

- Characterization of oxide films on service-exposed Zr-alloy components (oxide and crud morphology and associated water retention are important model inputs if energy deposited in the ZrO_2 is transferred to the adsorbed water). While not included in the FY22 test scope, service-exposed clad samples are anticipated to be addressed in a FY23 test series.

- Quantification of the amount of physisorbed (and chemisorbed, if any) water on ZrO_2 under relevant temperature and humidity conditions.
- Assessment of how much water is removed by the drying process, and
- Measurement of the G_{H2} for the same mini-canister setup containing only helium at controlled humidity to capture the contributions attributable to water vapor and physisorbed water on the stainless steel of the canister.

4.2. Test Approach

4.2.1. Zirconium samples and ZIRLO samples

The test approach will include preparation of zirconium and ZIRLO oxidized under controlled conditions. The use of uncontaminated surrogate samples rather than service-exposed cladding material avoids complications associated with performing testing on contaminated material and enables head-to-head comparison of otherwise-identical samples with different oxide thicknesses, alloys, etc., to investigate the impacts on radiolysis. The challenge is in ensuring samples that are sufficiently representative for single-effects type testing to draw useful conclusions.

Because the proposed test plan aims to systematically observe the impact of different factors relative to predicting radiolytic hydrogen generation, such as the impact of oxide thickness, substrate thickness, and replenishment of surface water, the primary goal is to produce samples in a way that allow these factors to be tuned without introducing unnecessary confounding variables, rather than to exactly reproduce the oxide condition on a service-exposed oxide surface.

If possible, testing in FY23 will also include de-fueled samples of service-exposed Zr-alloy cladding from the Sibling rod program. Such samples would enable characterization of the oxide present on actual cladding materials and potentially radiolysis testing of service-exposed samples to confirm that the radiolysis behavior is consistent with that obtained from the lab-produced surrogates. The testing of in-reactor generated oxide and crud will also provide data on retained water volume after drying that is an important modeling input.

4.2.2. Drying effectiveness

A drying process will be implemented to reduce/remove surface-adsorbed water from the samples prior to irradiation, in order to replicate the condition of cladding in SNF-in-canister conditions. The selection of drying conditions will be targeted to replicate the expected temperatures reached by the cladding and the vacuum duration of a realistic SNF drying process as implemented on the HBU Demo Cask.

4.2.3. ZrO_2 impact on radiolysis of adsorbed water

The previous analysis [d'Entremont et al., 2020b] assumed that due to energy transfer from the relatively thick ZrO_2 film, radiolysis of water adsorbed on ZrO_2 was accelerated relative to the water vapor in the canister, the water chemisorbed as hydrates on the aluminum alloy surfaces, and water that was physisorbed on the steel surfaces.

To test this assumption, the mini-canister setup will be irradiated with no Zr samples inside (only helium and controlled humidity) and then while loaded with lab-oxidized Zr surrogates providing large surface area under the same temperature and humidity conditions, in order to determine whether the hydrogen generation rate is greater in the presence of the Zr coupons. If the radiolysis rate in the presence of Zr surrogates is significantly higher than that of the empty canister under nominally identical conditions, it supports the hypothesis that radiolysis of water adsorbed on the coupon surfaces is indeed accelerated relative to water vapor.

The model developed previously [d'Entremont et al., 2020b] predicts that even a thin (e.g., 2 micron) ZrO_2 film would dramatically accelerate the radiolysis compared to direct radiolysis of the water vapor (estimates discussed in more detail in a later section), so the impact of the ZrO_2 should be observable within the planned irradiation schedules.

4.2.4. Energy transfer from oxide and/or metal

The previous analysis [d'Entremont et al., 2020b] assumed that all energy deposited in the ZrO_2 layer plus the energy deposited directly in the adsorbed water layer contributes to radiolysis of the surface-adsorbed water. Energy deposited in the metal substrate was not assumed to contribute to radiolysis.

- To test the former assumption, the ratio of oxide mass to adsorbed water mass will be varied by oxidizing samples to produce oxide films of at least two different thicknesses on otherwise nominally identical samples.
- To test for an impact of the metal substrate, the ratio of metal mass to oxide and adsorbed water mass will be varied by preparing coupons of at least two different thicknesses with the same oxidation procedure to produce nominally identical oxide films.
- These samples will be tested under nominally identical conditions (humidity, temperature, etc.) to determine whether the hydrogen production from the surface-adsorbed water varies with the mass of either the oxide or the metal.

4.2.5. Physisorbed water replenishment from humidity

The previous analysis [d'Entremont et al., 2020b] assumed that an equilibrium may be established between the surface-adsorbed water and the water vapor in the gas, so that surface-adsorbed water consumed by radiolysis can be replenished from the vapor until both sources are exhausted. Replenishment of surface-adsorbed water under radiolysis will be tested by comparing the measured evolution of H_2 and water vapor in the canister gas for canisters with and without Zr coupons.

Irradiation of an empty mini-canister backfilled with helium with water vapor will provide a baseline value for the H_2 generation rate associated with only water vapor and the steel surfaces, which is expected to be low. Irradiation of a mini-canister loaded with the Zr coupon assembly is expected to significantly accelerate the H_2 production, and either H_2 production far in excess of the expected loading of H_2O on the Zr surfaces *or* a significantly faster drop in the water vapor concentration would indicate that the water vapor is breaking down on the ZrO_2 surfaces.

Direct testing of the amount and speed of physisorption from humidity onto ZrO_2 surfaces under different temperature and humidity conditions may also be pursued as a supplement to the radiolysis tests, since the mini-canister testing will be limited to a small number of extended irradiation tests and cannot explore the full parameter space of interest.

5. EXPERIMENTAL SETUP AND METHODS

5.1. Gamma Irradiator

The gamma irradiation studies will be performed using a JL Shepherd Model 484 Co-60 irradiator, with a 10-inch by 10-inch irradiator cavity and present source strength providing maximum dose rates of ~0.5 Gy/s [McNamara and Verst, 2020a]. Note that the maximum irradiator dose rate is consistent with that assumed in the previous analysis, 3×10^{15} eV/g/s $= 0.48$ Gy/s [d'Entremont et al., 2019b]. The irradiation time will be selected to yield the desired total absorbed dose (as stated previously, measured G_{H2} values appear to be a function of dose, independent of dose rate).

As in the previous mini-canister testing [McNamara and Verst, 2020a], the vessels will be sized to allow for simultaneous irradiation of two mini-canisters side-by-side equidistant from the source. Final dose rates will be determined through radiation transport modeling to account for vessel placement and self-shielding.

As previously discussed, the temperatures in a dry storage canister are relatively high (Figure 3-1), and temperature could potentially impact the radiolytic H_2 generation by directly impacting the G_{H2} (Figure 2-1) and/or impacting the amount of surface-adsorbed water. The irradiator ambient temperature is only about 23.5°C. However, previous irradiation experiments in sealed ampoules were conducted at 100°C and 200°C using an insulated container and heating tapes inside the irradiator cavity [Parker-Quaife et al., 2019]. A similar approach is planned here in order to conduct the mini-canister tests at realistic canister temperatures (200–250°C). The insulation requirements will constrain the size of the canister feasible for elevated-temperature testing; it is anticipated based on previous experience that a ~5-inch tall mini-canister would allow sufficient space for insulation to maintain 250°C.

5.2. Mini-Canister and Instrumentation System

The testing described here will use an adaptation of an existing, proven mini-canister experimental setup. The mini-canister radiolysis testing system was designed and created to measure radiolytic gas generation from (oxy)hydroxide-bearing aluminum surrogates and to evaluate performance of a sensor system for extended, intermittent sampling of a sealed canister as part of a proposed dry-storage demo for research reactor fuel [McNamara and Verst, 2020a]. The system is designed to allow repeated, in-situ sampling of the same samples during a single continuous sample irradiation, rather than getting only one data point per sample-irradiation in a sealed-capsule irradiation. The use of a helium-filled steel canister also provides a close analogue to the environment of an actual dry-storage canister.

5.2.1. Mini-Canister

The mini-canister vessel will consist of a commercially available vacuum vessel sized to fit inside the irradiator cavity along with any thermal insulation needed to maintain it at elevated temperature during irradiation. The vessel will be connected to the testing manifold with a valve system allowing the gas inside to be sampled without moving or opening the vessel.

For the aluminum radiation tests in the mini-canister, the volumetric average dose rate inside the steel vessel was calculated to be $50\ \mathrm{krad/hr} = 0.14\ \mathrm{Gy/s}$ [Verst et al., 2020].

5.2.2. Sampling Instrumentation

To extract a gas sample, a dry scroll pump will evacuate the tubing before the sampling valve is opened, creating a differential pressure [McNamara and Verst, 2020a]. The test vessel contents will be allowed to equilibrate with the instrumentation manifold prior to measurement [McNamara and Verst, 2020a]. The gas sample volume will be determined by the length of the tubing and evaluated prior to testing [McNamara and Verst, 2020a]. Selection of the sampling frequency will take the container volume and manifold (gas sample) volume into account. A He backfill mechanism may be used to compensate for the removal of sampled gas and maintain the pressure [McNamara and Verst, 2020a].

The composition of gas samples drawn for analysis will be measured by a gas chromatograph (GC) based on calibration using known gas mixtures of H_2, N_2, and O_2 in helium balance, as performed in [McNamara and Verst, 2020a].

5.2.3. Helium Backfill

The helium backfill pressure will be 2.2 bar, replicating the pressure of the HBU Demo Cask [Bryan, 2019b]. The backfill will also include a controlled water vapor concentration depending on the parameters for the current test.

5.2.4. Canister Heating for Radiolysis at Elevated Temperature

Previous irradiations in the mini-canister setup were conducted at ambient temperature with a canister sized to maximize use of space in the irradiator cavity. Due to the relatively high temperature of commercial SNF [Fort, 2019], radiolysis testing at elevated temperature (up to ~250°C [Fort, 2019]) is important for obtaining data under realistic environmental conditions.

A heated test vessel containing individual sealed ampoules for radiolysis samples has been previously implemented in the irradiator using heating tape on the vessel exterior with thermal insulation around the vessel and heating tape to protect the irradiator. A similar approach will be used to heat the mini-canister for the planned test campaign. The dimensions of the mini-canister will be adjusted to allow room for the heating tape and thermal insulation around the canister.

5.3. Zr-alloy samples

5.3.1. Lab-prepared surrogate samples

Samples will be prepared out of both unalloyed zirconium and ZIRLO tubes available at SRNL. The unalloyed zirconium will provide baseline radiolytic yields independent of the effects of alloying elements such as Nb and facilitate more versatile sample preparation: Similar sample assemblies can be made with varying substrate thicknesses, and thicker oxide films can be more readily grown compared to the corrosion-resistant cladding alloy. The ZIRLO samples will provide data for a common cladding alloy and provide insight into the impact of the alloy on the radiolytic behavior.

For unalloyed zirconium, the coupon assembly design will be based on the previous mini-canister aluminum-coupon tests [McNamara and Verst, 2020b] and shown in Figure 5-1 and Figure 5-2, axially shortened to fit in the shorter canister. This coupon assembly was designed to maximize coupon area within the test vessel. It consists of a series of rectangular plates with widths varying based on location in the assembly, so that the outer envelope of the assembly follows the shape of the canister. The plates are assembled using a single nut and bolt running through a hole in the center of each plate, with washers to provide spaces between the plates to maintain consistent gaps.

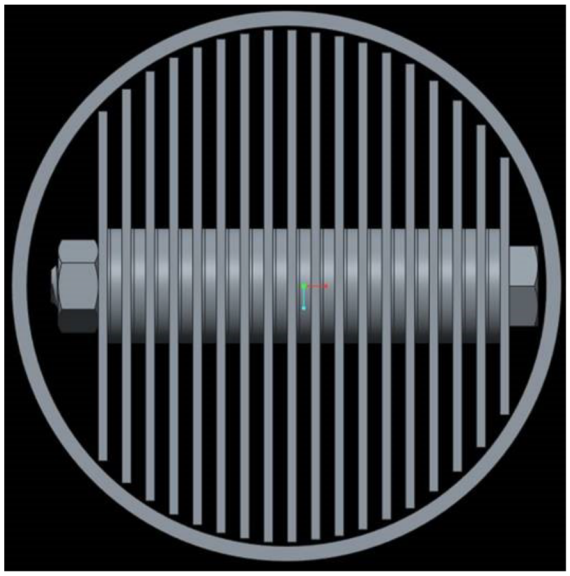

Figure 5-1. Schematic of coupon assembly design from [McNamara and Verst, 2020b], viewed from the top.

Figure 5-2. Photos of aluminum coupon assembly and corresponding mini-canister from [McNamara and Verst, 2020b]. The proposed sample design will be similar for the oxidized unalloyed Zr material, but axially shortened to accommodate thermal insulation around the mini-canister. Oxidized ZIRLO tubes would be used in a separate mini-canister.

The ZIRLO tubing has nominal dimensions of 9.52 mm outer diameter and 8.38 mm inner diameter (0.57 mm wall thickness), in lengths greater than the height of the mini-canister. The layout of ZIRLO samples in the mini-canister is yet to be determined, but will most likely consist of a packing of ZIRLO tube sections slightly smaller than the internal height of the mini-canister, with some form of spacers to maintain gaps between adjacent tubes. Both sides of the Zr tube wall will be exposed. The number of tube sections that will fit within the mini-canister cross section will depend on the packing and spacer arrangement chosen.

The Zr sheet samples and ZIRLO tube sections will be air oxidized. The exact exposure parameters will be initially determined to produce oxide films ranging from 2 microns to about 10 microns. For this test series the focus is on generating basic data using a sufficient oxide mass to achieve surface water removal by radiolysis in an optimum exposure time. The effects from different oxide morphologies between lab generated and in-service grown oxides will be characterized when in-service samples are available.

5.3.2. Service-exposed materials (FY23)

The physical characteristics of high burnup fuel rods with relatively thick oxides (and with crud) are not easily duplicated by lab-grown surrogates. To obtain the most relevant data to verify how lab-grown surrogates compare to service-exposed materials and whether the radiolysis results obtained from each are comparable, it is helpful to characterize and/or test actual fuel rod cladding samples. This plan assumes that samples from existing "sister" rods of the High Burnup Demo Cask rods can be obtained and used for a portion of the evaluations in FY23. The Zircaloy 4 and ZIRLO rods have the most oxide and crud and obtaining samples from these rods will be pursued. As available, samples from the M5 clad rods can also be included.

5.3.3. Sample characterization

Planned sample characterization includes:

- Weighing before and after oxidation of the sample assemblies, providing a measure of the amount of oxidation. Weighing before and after a sample drying process may also be conducted; however, since samples are planned to be weighed in-canister, the drying mass loss associated with each irradiation test will not be obtained.
- Scanning electron microscopy (SEM)of sample surfaces after oxidation to characterize the oxide morphology and of sample cross-sections to characterize oxide thickness. Similar SEM will be conducted on service-exposed materials for comparison, if obtained for FY23 testing.
- X-ray diffraction (XRD) will be performed after sample oxidation to confirm formation of ZrO_2 and negligible hydrated species. Similar characterization will be performed for service-exposed materials, if obtained for FY23 testing.

5.4. Drying

In vacuum drying of SNF, the decay heat of the fuel itself ensures that the fuel reaches elevated temperatures during drying, and the elevated temperature, as well as the vacuum, is expected to play a key role in releasing physisorbed/chemisorbed water. Non-radioactive surrogate samples lack this internal heating, so simply applying the same vacuum steps is insufficient to replicate the drying process. In addition, externally heating samples during vacuum drying is complicated by the thermal insulation provided by the vacuum itself.

For the present test plan, the drying process will be similar to that used previously for the aluminum-clad SNF mini-canister tests [Verst et al., 2021]. Specifically, the coupons will be loaded into the mini-canister vessel; the loaded vessel will be placed in a furnace with a inlet tube leading outside the furnace and heated (in air) to a target temperature for a specified duration (4 hours at 220°C was used in the previous aluminum test), followed by pulling a vacuum while the vessel remains in the furnace at the same temperature. Multiple helium purges and an extended vacuum hold will be conducted prior to backfilling with helium (and humidity according to the test parameters) to the test pressure. This drying approach aims to separately achieve the effects of elevated temperature and vacuum exposure rather than trying to achieve both simultaneously.

The planned drying temperature is 220°C.

5.5. **Model estimates for mini-canister setup**

The anticipated radiolytic H_2 production for the mini-canister setup can be estimated using the same model and assumptions used in the analysis of the HBU Cask [d'Entremont et al., 2020b]. The proposed mini-canister is assumed to have internal height ~5 inches and internal diameter 2.83 inches. The surface area and volume of the coupon assembly are approximated based on the design of the Al coupon assemblies tested previously [McNamara and Verst, 2020b], scaled down based on the reduced height of the canister, yielding an estimated nominal sample surface area of ~2580 cm^2 and volume of ~230 cm^3. Using an estimated average temperature of 200°C and the ideal gas law, the 2.2 bar He backfill yields an estimated 0.016 mol He in the mini-canister.

The only H_2O sources in this analysis are the water adsorbed to the surfaces of the steel canister and Zr coupon assembly and the water vapor. The lab-grown ZrO_2 is assumed to have negligible fissuring and no crud, so only the nominal surface-adsorbed water for ZrO_2 is included in the estimate. The dose rate inside the mini-canister is taken as 0.14 Gy/s, based on the value calculated for the previous mini-canister testing. Using the assumptions from Ref. [d'Entremont et al., 2020b] for the water loading and assuming 20000 ppmv initial water vapor at 200°C, the total estimated H_2O in the canister is 3.3×10^{-4} mol, including 1.3×10^{-5} mol associated with the ZrO_2 surface.

Using the G_{H2} values assumed in Ref. [d'Entremont et al., 2020b] and assuming 39 microns of ZrO_2 (as used in the previous analysis), the 0.14 Gy/s irradiation is predicted to consume the water initially adsorbed on ZrO_2 within 10 hours (producing 808 ppmv H_2) and consume all water within the canister within 10 days (producing 20800 ppmv of H_2) given replenishment. By contrast, the model predicts that direct radiolysis of the water vapor without interaction with ZrO_2 (i.e., the empty-canister setup) would take ~1.3 years to produce just 100 ppmv of radiolytic H_2 and >250 years to consume all of the water vapor (assuming a constant H_2 generation rate, which would not be the case for water vapor due to the decrease in H_2O mass to absorb the dose).

Realistically, producing samples of cladding alloys with 39 μm thick surface oxide layers is expected to be infeasible without excessively long sample preparation. With current model assumptions, the predicted rate of radiolysis of ZrO_2-adsorbed water is directly proportional to the thickness of the ZrO_2, so thinner oxides will extend the amount of time required to consume the water. Assuming 10 μm of ZrO_2 on the coupon surfaces, the initial surface-adsorbed water on the ZrO_2 is predicted to be consumed in about 1.5 days and all water in the canister consumed in under 40 days with replenishment. Assuming 2 μm of ZrO_2, consumption of the initial surface-adsorbed water on ZrO_2 is predicted to take about 8 days and all water in the canister consumed in about 194 days with replenishment.

The previous mini-canister setup was able to detect H_2 down to 100 ppmv. Based on the model predictions,

- Zr-coupon-loaded tests with even relatively thin oxide layers (1–2 microns) are predicted to generate measurable amounts of H_2 within a few days of irradiation. Assuming similar sensitivity can be achieved for H_2O, measurable depletion of the water vapor in the case of surface replenishment *or* exhaustion of the ZrO_2-adsorbed water in the absence of replenishment is predicted to be achievable within several weeks of testing.
- Thicker oxides (e.g., 5–10 microns) should enable reaching a plateau of H_2 concentration within several months via either complete exhaustion of the H_2O in the canister or reaching an equilibrium state between radiolytic production and consumption via back-reactions or gettering.
- H_2 generation and water vapor depletion in the absence of Zr-alloy surfaces (the "empty-canister" condition) are expected to be too slow to achieve measurable H_2 generation results in a

reasonable test duration, but will provide a baseline data point and characterize the impact of steel surfaces on the hydrogen generation rates as significant or not.

6. PRELIMINARY TEST MATRIX

The table below reflects the test conditions for radiolysis testing. The primary variables are:

- Substrate material: Unalloyed zirconium and ZIRLO
- Oxide thickness: Two different thicknesses (values will depend on results of oxidation tests; 2 and 10 μm are tentative targets.)
- Water vapor condition: Two different conditions, dry helium backfill and 20000 ppmv water vapor in helium

The "no water vapor" condition will be targeted to have nominally zero water vapor (dry helium cover gas) and be dried using the same drying procedure as the baseline tests in order to capture the H_2 generation associated with only the surface-adsorbed water retained through the drying process (the water vapor in other tests is expected to represent water vapor that may be retained in other areas of an SNF-in-canister).

This matrix will be further reviewed and updated prior to commencement of testing at the start of FY22.

	Substrate Material	**Substrate thickness**	**Oxide thickness**	**Water vapor (in He gas)**	**Irradiation Temperature**
Empty canister	N/A	N/A	N/A	20000 ppmv	200°C
Baseline (baseline G_{H2})	Zr	Baseline	Baseline	20000 ppmv	200°C
Different oxide thickness	Zr	Baseline	Different (probably smaller)	20000 ppmv	200°C
Different substrate thickness	Zr	Thicker	Baseline	20000 ppmv	200°C
No water vapor	Zr	Baseline	Baseline	Nominally 0	200°C
ZIRLO	ZIRLO	0.57 mm	Baseline	20000 ppmv	200°C

If service-exposed materials are obtained for testing in FY23, additional radiolysis tests would be conducted with the service-exposed material. The test matrix for this additional testing will depend on the samples available.

7. CONCLUSIONS

A "mini-canister" or small stainless steel vessel will be loaded with high-surface-area Zr or ZIRLO surrogate samples (with appropriate lab-grown surface oxide) and vacuum-dried using a procedure designed to replicate the expected temperatures and vacuum exposure of SNF-in-canister drying. The inventories of water associated with the materials will be quantified based on the prior estimation scheme [d'Entremont, 2020b]. The mini-canister will be staged in a ^{60}Co irradiator for radiolysis testing with controllable heating and controllable initial humidity and on-line periodic sampling of the gas space to provide characterization of the H_2 and H_2O evolution. This test system and modeling thereof will provide information to refine the prediction of radiolysis associated with Zr-alloy components in SNF canisters containing residual water.

8. REFERENCES

Agayev, T. N., Faradj-zadeh, I. A., Aliyev, A. G., Eyubov, K. T., & Aliyev, S. M. (2017). "Regularities of radiation and heterogeneous processes in contact of Zr and Zr1% Nb alloy with water". Вопросы атомной науки и техники.

Arkhipov, O. P., Verkhovskaya, A. O., Kabakchi, S. A., & Ermakov, A. N. (2007). Development and verification of a mathematical model of the radiolysis of water vapor. Atomic energy, 103(5), 870-874.

ASTM International. "Standard Guide for Drying Behavior of Spent Nuclear Fuel." ASTM C1553–16. West Conshohocken, Pennsylvania: ASTM International. 2016.

Bryan, Charles, Russell Jarek, Chris Flores, Elliott Leonard: High Burn-up Demonstration Cask: SNL Gas Analyses: Sandia National Laboratories ASTM Nuclear Fuel Drying Workshop January 29, 2019a; also in SNL report Bryan, Charles R., Russell L. Jarek, Chris Flores, Elliott Leonard, Analysis of Gas Samples Taken from the High Burnup Demonstration Cask, Sandia National Laboratories, SANDIA REPORT SAND2019-2281.

Bryan, C.R., S.G. Durbin, E. Lindgren, A.G. Ilgen, T.J. Montoya, T. Dewers, D. Fascitelli. "SNL Contribution: Consequence Analysis for Moisture Remaining in Dry Storage Canisters After Drying," Sandia National Laboratory, SAND2019-8532 R, 2019b.

CNWRA. Extended Storage and Transportation: Evaluation of Drying Adequacy. Authors: H. Jung, P. Shukla, T. Ahn, L. Tipton, K. Das, X. He, and D. Basu, San Antonio, Texas: Center for Nuclear Waste Regulatory Analyses. 2013.

d'Entremont, A. L., Fuentes, R. E., Shalloo, M. G., Knight, T. W., Sindelar, R. L., "Thermal Dehydration of Aluminum (Oxy)hydroxides on Fuel Cladding Material," Proceedings of Waste Management Symposia 2020, #20200, 2020a.

d'Entremont, A. L., Kesterson, R. L., Sindelar, R. L., "Evaluation of Hydrogen Generation in High Burnup Demonstration Dry Storage Cask," SRNL-STI-2020-00268, 2020b.

d'Entremont, A. L., Olson, L. C., Verst, C. G., Fuentes, R. E., Sindelar, R. L., "(Oxy)hydroxides Formed on Aluminum Fuel Materials After Irradiation and Long-Term Wet Storage," Proceedings of Waste Management Symposia 2020, #20354, 2020c.

Dylla, H.F.; "The Problem of Water in Vacuum Systems", presentation at CERN Accelerator School May 2006

Elliot, A. J., and D. M. Bartels. "The reaction set, rate constants and g-values for the simulation of the radiolysis of light water over the range 20° to 350°C based on information available in 2008". No. AECL—153-127160-450-001. Atomic Energy of Canada Limited, 2009.Fort, James A., D.J. Richmond, J.M. Cuta, S.R. Suffield, "Thermal Modeling of the TN-32B Cask for the High Burnup Spent Fuel Data Project", July 30, 2019, PNNL-28915

Garibov, A.A., T.N. Agayev, G.T. Imanova, K.T. Eyubov, "Kinetics of radiation and catalytic decomposition of water in the presence of nano-zirconium dioxide." issn 1562-6016. PAST. 2015. №5(99), p. 48.

Holmes, H. F., Fuller Jr, E. L., & Beh, R. A. (1974). "Adsorption of argon, nitrogen, and water vapor on zirconium oxide". Journal of Colloid and Interface Science, 47(2), 365-371.

Kabakchi, S.A.,O.P. Arkhipov, M.L. Lukashenko: " Specific Features of the Radiolysis of Water and Aqueous Solutions of H2 and O2 by Mixed n,γ-Radiation with a High Portion of the Neutron Component.", High Energy Chemistry 47, 2013, 147-151.

Knoll, R.W., et al., “Evaluation of Cover Gas Impurities and Their Effects on the Dry Storage of LWR Spent Fuel,” PNL-6365, DE88 003983, Pacific Northwest National Laboratory, November 1987.

Köck, E. M., Kogler, M., Klötzer, B., Noisternig, M. F., & Penner, S. (2016).” Structural and electrochemical properties of physisorbed and chemisorbed water layers on the ceramic oxides Y2O3, YSZ, and ZrO2”. ACS applied materials & interfaces, 8(25), 16428-16443

Le Caër, S.; " Water Radiolysis: Influence of Oxide Surfaces on H2 Production under Ionizing Radiation", Water 3, 2011, 235-253.

McNamara, J., Verst, C., “Aluminum Spent Nuclear Fuel 2020 Large Sample Radiolysis and Measurement Test Plan,” SRNL-RP-2020-00219, 2020a.

McNamara, J., Verst, C., “Instrumented Lid – Fabricate Hydrated Oxide Specimens for Testing,” SRNL-L6000-2020-00034, 2020b.

Parker-Quaife, E. H., Horne, G. P., “Milestone 2.8: Preliminary Radiolytic Gas Generation Measurements from Helium-Backfilled Samples,” INL/EXT-21-61404-Rev000, 2020.

Parker-Quaife, E. H., Horne, G. P., Heathman, C. R., Verst, C., Zalupski, P. R., “Radiation-Induced Molecular Hydrogen Gas Generation by Pre-Corroded Aluminum Alloy 1100,” INL/EXT-19-55202, 2019.

Petrik, N. G., Alexandrov, A. B., & Vall, A. I. (2001).” Interfacial energy transfer during gamma radiolysis of water on the surface of ZrO2 and some other oxides”. The Journal of Physical Chemistry B, 105(25), 5935-5944.

Shukla, P, R.L. Sindelar, P.-S. Lam, “Consequence Analysis of Residual Water in a Storage Canister – Preliminary Report,” SRNL–STI–2019–00495

Sindelar, R.L., M.J. Connolly, J.J. Jarrell, D.T. Herman, and W.H. Bates, *Technology Development for Dry Storage of Aluminum-Clad Spent Nuclear Fuel*, Paper 20490 at WM2020, March 2020.

Skotnicki, K., & Bobrowski, K.; “Molecular hydrogen formation during water radiolysis in the presence of zirconium dioxide.” Journal of Radioanalytical and Nuclear Chemistry, 304(2), 473-480. (2015)

Spinks,J. W., Woods, R.J.; "An Introduction to Radiation Chemistry", 3rd ed., Wiley Interscience, New York, 1990.

Verst, C., Randall, B., McNamara, J., “Instrumented Lid – Initiation Irradiation and Measurement of As-Is Hydrated Oxide Specimens (Large Coupons),” SRNL-L6000-2020-00038, 2020.

Verst, C., d’Entremont, A., Randall, B., McNamara, J., “Interim Irradiation and Measurement of As-Dried Vs As-Corroded Hydrated Oxide Specimens (Large Coupons),” SRNL-L6000-2021-00006, 2021.

Wang, M.; " Irradiated Assisted Corrosion of Stainless Steel in Light Water Reactors" – Focus on Radiolysis and Corrosion Damage. hal-00841142, 2013

Wertsching, A. K. "Material Interactions on Canister Integrity during Storage and Transport." DOE/SNF/REP-104 (2007)

Wittman, R.S.; "Radiolysis Model Sensitivity Analysis for a Used Fuel Storage Canister", FCRD-UFD-2013-000357, PNNL-22773, 2013.